2-15-1998

A Model for Calculating Acoustic Gravity Wave Energy and Momentum Flux in the Mesosphere from OH Airglow

Gary R. Swenson

Alan Z. Liu
Embry Riddle Aeronautical University - Daytona Beach, liuz2@erau.edu

GEOPHYSICAL RESEARCH LETTERS, VOL. 25, NO. 4, PAGES 477-480, FEBRUARY 15, 1998

A model for calculating Acoustic Gravity Wave energy and momentum flux in the mesosphere from OH airglow

Gary R. Swenson and Alan Z. Liu

University of Illinois, Dept. of Electrical and Computer Engineering, Urbana

Abstract. Acoustic gravity and tidal waves propagating in the mesosphere/lower thermosphere (80-110 km) perturb the airglow layer intensities. The OH airglow has recently been modeled to determine the relationship between the relative perturbed atmospheric density and temperature (ρ'/ρ, T'/T) to the OH intensity (I'_{OH}/I_{OH}) at the OH emission altitudes [Swenson and Gardner, 1997]. A model is presented here which relates wave perturbed OH airglow to the wave energy and momentum flux as they propagate through the emission layer. The model is dependent on the wave horizontal and vertical wavelengths (or phase speed as related through the dispersion relationship), and the relative perturbed airglow intensity, I'_{OH}/I_{OH}. The model can be used by optical experimenters to relate their measurements to wave energy and momentum flux in the stated altitude region.

Introduction

The influence of Acoustic Gravity Waves (AGWs) on the dynamics in the mesosphere is a major consideration in GCM modeling. Parameterization and a description of the current understanding of AGW effects in the mesosphere/lower thermosphere has been described by several models including Fritts et al. [1993] and Fritts and Lu, [1993]. Fritts and Lu [1993] predict deceleration of up to several 100's ms^{-1} day^{-1} in the winter mesosphere, and large seasonal contrasts as a result of momentum effects of AGWs. Vincent [1984] describes a spectral study of MF radar data from two stations (Adelaide and Townsville) for a large temporal spectral range (0.1-20 hours) and finds most (75%) of the wave energy flux content from AGWs is in those waves with a period (τ) < one hour. Airglow imagers viewing the mesosphere are uniquely equipped to view a large area of atmosphere with allsky optics, nominally to 300-400 km radius from ground stations. The predominant AGW waves observed by airglow imagers are those with a large vertical wavelengths. These waves are the fast, short period waves which fall into the portion of the spectrum identified by Vincent [1984] as carrying most of the wave energy flux content which has influence on the large scale dynamics in this atmospheric region.

Extracting dynamical quantities from airglow observations has been explored by several modeling activities, one of which is described by Battaner and Molina [1980]. They studied the kinetic energy density of waves in the OI 557.5 nm airglow to investigate the vertical eddy diffusion transport from the seasonal occurance of waves observed in the layer. As our measurement technology enables us to establish the intrinsic wave parameters, we can better infer the wave energy and momentum flux in the upper mesosphere region.

Methods have been developed to extract the directional spectral content of OH image data [Gardner et al., 1996]. A complete spectral treatment of the wave energy and momentum in the airglow is being developed, but the main focus of this initial study is the monochromatic waves. Monochromatic waves with horizontal wavelength (λ_x) of 20-30 km and phase speeds in the 40-70 ms^{-1} range dominate [for example see Taylor et al. 1987, and Swenson and Mende, 1994]. Swenson and Gardner [1997] have developed the relationship between the OH airglow intensity perturbation and the atmospheric temperature/density disturbance due to waves. With this information, the energy/momentum flux equations can be derived in terms of the intensity perturbations observed in OH and the intrinsic wave parameters. This is of particular interest since:

1) The monochromatic wave fluxes are often planar, and propagate in a particular azimuth direction. For vertically propagating waves, the vertical momentum flux divergence will act to decelerate the mean flow in the mesosphere.

2) New measurement methods of T, ρ, and u, v, w using lidar in the mesosphere will be able to measure directly the momentum flux over long time periods. The magnitude of the flux component due to the monochromatic waves observed in airglow can be compared to the total flux measured by lidar, radar, and other methods.

3) Future experiments on the NASA TIMED satellite will be able to make energy and momentum balance in the mesosphere. The very large component of AGW energy and momentum flux through a fixed altitude using this method can contribute to those studies.

4) This method is also applied to the other mesosphere/lower thermosphere airglows which originate at higher altitudes than OH. The flux divergence between the layers can be measured, and the associated mean deceleration (acceleration) due to the observed waves can be calculated. Since the OH and O_2 Atmospheric Band layers are separated by 6 km, the mean deceleration due to these waves can be measured for the 87 - 93 km region. OI (557.7 nm) and Na (589.2 nm) airglows may also be studied to extract similar information.

Energy and Momentum Flux Model

Monochromatic waves at a fixed altitude can be represented as

$$\rho'/\rho = -T'/\overline{T} = \varepsilon \cdot e^{\beta(z-z_{OH})} \cdot \cos\left[\omega t - kx + m\left(z - z_{OH}\right)\right], \quad (1)$$

where $\mathrm{var}(\rho'/\rho) = \mathrm{var}(-T'/\overline{T}) = \langle(\varepsilon \cos[])^2\rangle \cong 0.5\,\varepsilon^2$ is the wave amplitude at altitude z_{OH}, ω is the intrinsic frequency, $m = 2\pi/\lambda_z$ is the vertical wave number, $k = 2\pi/\lambda_x$ is the horizontal wave number, λ_z = vertical wavelength, λ_x = horizon-

Paper number 98GL00132.
0094-8534/98/98GL-00132$05.00

tal wavelength, $\overline{T}$ = undisturbed atmospheric temperature and T' = the component of temperature resulting wave disturbance. The frequency and wave numbers are related through the dispersion relation:

$$m^2 = \frac{N^2 - \omega^2}{\omega^2 - f^2} k^2, \quad (2)$$

where N is the Brunt Vaisala frequency and f is the inertial frequency. In the case where $N^2 >> \omega^2 >> f^2$, which is the case for wave period of 15 min ~ 1 hour in the mesosphere, (2) reduces to

$$\lambda_z = \frac{\lambda_x}{\tau_I} \tau_{BV} = C_I \cdot \tau_{BV}, \quad (3)$$

where τ_{BV} and τ_I are the Brunt Vaisala and intrinsic wave periods and C_I is the intrinsic phase speed.

Given the measurement of the AGW intrinsic characteristics, one can compute the wave energy (momentum) flux for the wave. Gravity wave energy flux may be written [see Vincent, 1984]:

$$F_E = \frac{-\rho_0 \lambda_z^2 g^2}{\lambda_x \tau_{BV} N^2} \left\langle \left(\frac{T'}{\overline{T}} \right)^2 \right\rangle, \quad (4)$$

where ρ_0 is the mass density. It follows that the momentum flux is given by:

$$F_M = \frac{\lambda_z}{\lambda_x} \frac{g^2}{N^2} \left\langle \left(\frac{T'}{\overline{T}} \right)^2 \right\rangle. \quad (5)$$

The consideration here is to calculate the flux at 87 km, the altitude at which the variance in OH is maximum due to wave disturbances [Swenson and Gardner, 1997]. The MSIS model atmosphere [Hedin, 1991] density ($5.6\ 10^{-6}$ kg m^{-3}) and associated temperature results in, τ_{BV} = 300 s, and N = 0.02 rd s^{-1}, which reduces (4) to:

$$F_{E,87km} = -\frac{C_E \lambda_z^2}{\lambda_x} \left\langle \left(\frac{T'}{\overline{T}} \right)^2 \right\rangle \ \left(Wm^{-2} \right), \quad (6)$$

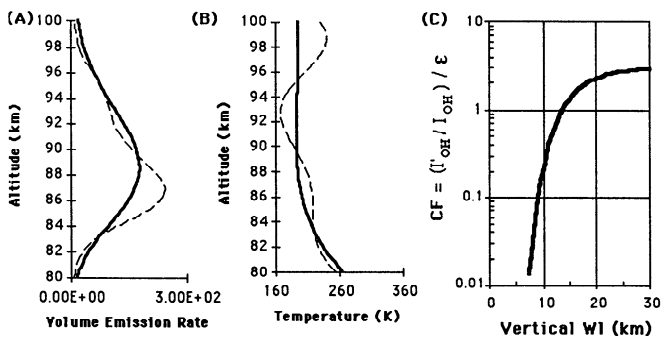

Figure 1. (A) and (B) solid are the undisturbed volume emission rate and MSIS 90 temperature profile and the dashed is an exemplary wave at a random phase, with λ_z = 10 km. The particular wave is undamped so the amplitude increases with altitude at a rate equal to the equivalent decrease in density so that the energy flux is constant. As the volume emission profile is integrated over altitude in (A) for all phases of the wave, the effective I'_{OH}/I_{OH} can be calculated for the range of λ_z. (C) is a plot of the ratio of the integrated volume emission rate I'_{OH}/I_{OH} to wave amplitude ε, versus λ_z.

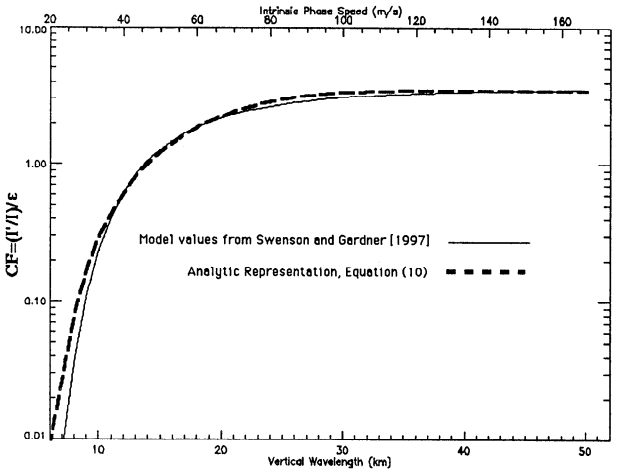

Figure 2. A plot of the cancellation factor (CF) for OH intensity versus λ_z from Swenson and Gardner [1997], for undamped AGWs (thin line), and an analytic representation from equation (10), (thick dashed linc.)

and consequently, the momentum flux is:

$$F_{M,87km} = \frac{C_M \lambda_z}{\lambda_x} \left\langle \left(\frac{T'}{\overline{T}} \right)^2 \right\rangle \ \left(m^2 s^{-2} \right), \quad (7)$$

where $C_E = (5.6 \cdot 10^{-6} kg m^{-3} \cdot 96 m^2 s^{-4}) / (300 s \cdot 0.0004 rd^2 s^{-2}) = 4.5 \cdot 10^{-3} kg m^{-1} s^{-2} rd^{-2}$ and $C_M = (96 m^2 s^{-4}) / (0.0004 rd^2 s^{-2}) = 2.4 \cdot 10^5 m^2 s^{-2}$ are the constants for the mks units indicated.

The objective here is to relate the perturbation parameter in the energy and momentum equations to the airglow intensity. Swenson and Gardner [1997] have characterized the relationship of monochromatic atmospheric density/temperature perturbations to the OH integrated volume emission rate of the layer as described in Figure 1. The OH perturbations to the atmosphere are significantly attenuated at λ_z < 12 km. Figure 1(C) relates the dependence $(T'/\overline{T}) = (I'_{OH}/I_{OH})/CF$, where I_{OH} and I'_{OH} are volume integrated intensity for the undisturbed layer and the disturbed component, respectively, and CF is the cancellation factor from Swenson and Gardner, described in Figure 1(C). Note that the CF factor is relating the airglow intensity to the wave perturbed atmsopheric temperature, and is not to be confused with the Krassovsky factor η, which relates the intensity to the airglow, volume integrated brightness temperture [Krassovsky, 1972]. Using these relationships, equation (6) can be rewritten in terms of the perturbed OH volume emission rate and wave dimensions as:

$$F_{E,87km} = \frac{2.3 \cdot 10^{-3} \cdot \lambda_z^2 (I'_{OH})^2}{\lambda_x \cdot CF^2 (I_{OH})^2} \ \left(Wm^{-2} \right). \quad (8)$$

Momentum flux (7) can be combined with (8) to yield:

$$F_{M,87km} = \frac{6 \cdot 10^4 \lambda_z (I'_{OH})^2}{\lambda_x \cdot CF^2 (I_{OH})^2} \ \left(m^2 s^{-2} \right). \quad (9)$$

Note that the expression for momentum flux is independent of λ_x, but dependent on λ_z through CF. Equations (8) and (9) relate the energy and momentum flux to the wave amplitude (mean to peak) as described in expression (1), and not the variance. Equations (8) and (9) then are designed to calculate the fluxes for the magnitudes of monochromatic features, where

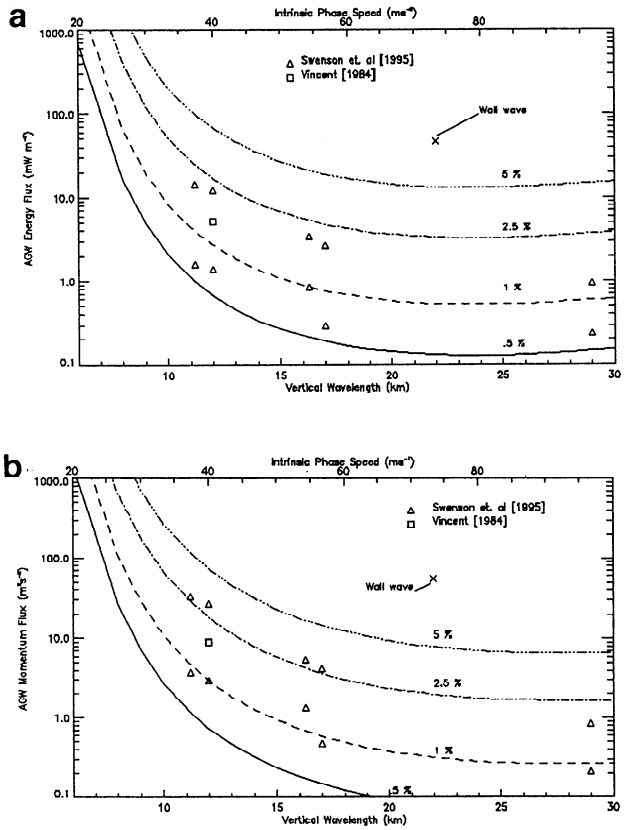

Figure 3. (A) Vertical wavelength versus gravity wave energy flux at an assumed altitude of 87 km for a range of perturbed OH volume emission rates including 0.5, 1, 2.5 and 5% for an assumed λ_x of 30 km. The I'_{OH}/I_{OH} changes are mean to peak changes associated with a monochromatic wave. The Δ's are data from intrinsic wave data and I'_{OH}/I_{OH} measurements by Swenson et al. 1995. The extreme 'wall' event (X) is discussed in the text. The energy and momentum flux for the data plotted incorporated the measured I'_{OH}/I_{OH}, λ_x, whereas λ_z was calculated from the measured intrinsic phase speed given the assumptions in equation (3). As a reference, the square represents the data average from Adelaide for Periods 0.1-0.5 hour from Vincent [1984] using MF radar where the data represented a number of months sampling at different seasons. (B) Same as (A), but momentum flux.

I'_{OH}/I_{OH} (mean to peak) can be measured. Expressions of flux considering spectral variance may be calculated using (6) and (7) as described above, but without the variance to amplitude relationship described from (1).

The cancellation factor can be represented as an exponential function, which has been best fit to the relationship generated by Swenson and Gardner [1997] for waves which are undamped as:

$$CF = 3.5 - (3.5 - 0.01)e^{-0.0055(\lambda_z - 6\text{km})^2}, \qquad (10)$$

where λ_z in (10) is in km. A comparison of the modeled and analytic representation from (10) is shown in Figure 2. The top scale in fig 2. relates the CF to phase speed, assuming the dispersion relationship shown in equation (3). The expression is valid for $\lambda_z \geq 6$ km, and for $\lambda_z < 6$ km the CF is extremely small, and I'/I is below threshold of being significant.

Discussion

A range of perturbations in I'_{OH}/I_{OH} are shown in Figure 3 for both energy flux using (8) and momentum flux using (9). Equations (8) and (9) are derived for I'_{OH} values as a mean to peak change associated with the wave.

It should be pointed out that the expressions presented include assumptions considering the waves extend through the altitude region to fill the OH emission layer. On occasion, the leading edge of propagating phase fronts, or single waves will be observed and will not have totally propagated through the layer, wherein the CF described here is not applicable.

Swenson and Gardner [1997] have validated the I'_{OH}/I_{OH} relationship shown in Figure 2 with measurements, for $\lambda_z > 12$ km. The detailed slope and the steepness of the cutoff to shorter wavelengths has not been validated. Estimates are that the uncertainties in the CF are <50% for $\lambda_z > 12$ km, but potentially larger at shorter λ_z. It is also pointed out that in many of the AGWs measured, τ_{BV} is not $<<$ τ_I, and often $\tau_I \sim 2\tau_{BV}$, which will introduce an error in the expression due to the assumptions made in dispersion relationship, equation (3). The error introduced for $\tau_I \sim 2\tau_{BV}$ is an underestimate of λ_z by 16%, which extends to an underestimate in F_E of ~35% and F_M of 16%.

Extracting intrinsic AGW parameters λ_x, λ_z (or intrinsic phase speed), and the associated intensity perturbation (I'_{OH}/I_{OH}) required for the calculations have been described for airglow images by Swenson et al. [1995] and Taylor et al. [1995]. Some representative data is included on Figure 3 from both 'typical' wave structure where λ_x is ~ 20-70 km as well as a large amplitude 'extreme' as reflected by the 'wall' event documented by Swenson et al. [1997] where the key parameters were I'_{OH}/I_{OH} ~30%, λ_x~300 km, and λ_z~20 km. These extreme events appear to be relatively rare. The 'typical' data shown is taken from ALOHA campaign [Swenson et al. 1995], where imagery and wind data were acquired, and intrinsic wave parameters were calculated. It is only recently that measurements are being made by correlative methods to document all the parameters including the winds, to make the calculation. The data presented here is only intended to be a sample to demonstrate the range of energy and momentum flux resulting from the measurements and calculations, and not to be considered as means. Long term measurements are now necessary to characterize the statistically meaningful values. We do have analysis in progress where quality wind measurements were made simultaneously, in the same local volume as observed phase speeds, which will be published in the near future.

Summary

An analytic expression has been developed which relates AGW energy and momentum flux to the intrinsic AGW parameters λ_x, λ_z (or intrinsic phase speed), and the associated intensity perturbation associated with the wave disturbed airglow (I'_{OH}/I_{OH}). Data currently acquired by imagers can establish λ_x, I'_{OH}/I_{OH}, and observed phase speed. Simultaneous measurements of winds at altitude from lidar, radar, or spacecraft are necessary to extract the intrinsic phase speed, from any observational platform. The dispersion relationship is used to calculate λ_z. Other methods, such as lidar and radar, can potentially measure λ_z directly.

The planar, monochromatic AGWs observed by imagers have a potentially major influence on mesosphere dynamics through the interaction and deceleration of the flow. Monochromatic features have a maximum impact when the phase propagation direction is in the plane of the wind. The effects of momentum transfer will depend on this alignment and consequently, wind vector information will be as important as the momentum flux in accumulating information on the drag resulting from AGWs.

The O_2 Atmospheric band lies ~ 6 km above the OH layer. Models of wave energy and momentum flux are being developed for this layer, similar to that presented here. With that information, the deduction of the wave energy (and momentum) flux divergence can be calculated. Consequently, the average momentum dissipation (per unit time) can be calculated from information of I′/I from both layers. This will evolve the capability to calculate the AGW wind loading (per unit time) for the region between the layers.

Acknowledgments. This work was supported in part by the National Science Foundation through the grant ATM 96-96246.

References

Battaner, E. and A. Molina, Turbopause internal gravity waves, 557.7 nm airglow, and eddy diffusion coeffiecient, *J. Geophys. Res.*, **85**, 6803-6810, 1980.

Gardner, C. S., M. Coble, G. C. Papen, and G. R. Swenson, Observations of the unambiguous two-dimensional horizontal wave number spectra of OH intensity perturbations, *Geophys. Res. Lett.*, **23**, 3739-3742, 1996.

Krassovsky, V. I., Infrasonic variations of the OH emission in the upper atmosphere, *Ann. Geophys.*, **28**, 739-746, 1972.

Fritts, D. C., and T. E. VanZandt, Spectral estimates of gravity wave energy and momentum fluxes, Part I: Energy dissipation, acceleration, and constraints, *J. Atmos. Sci.*, **50**, 3685-3694, 1993.

Fritts, D. C., and W. Lu, Spectral estimates of gravity wave energy and momentum fluxes, Part II: Parameterization of wave forcing and variability, *J. Atmos. Sci.*, **50**, 3695-3713, 1993.

Swenson, G. R., and S. B. Mende, OH emission and gravity waves (including a breaking wave) in all-sky imagery from Bear Lake, UT., *Geophys. Res. Lett.*, **21**, 2239-2242, 1994.

Swenson, G. R., M. J. Taylor, P. J. Espy, C. Gardner, and X. Tao, ALOHA-93 measurements of intrinsic AGW characteristics using airborne airglow imager and groundbased Na wind/temperature lidar, *Geophys. Res. Lett.*, **22**, 2841-2844, 1995.

Swenson, G. R. and C. S. Gardner, Analytical models for the responses of the mesospheric Na and OH* layers to atmospheric gravity waves, *J. Geophys. Res.-Atmos*, In Press, 1998.

Swenson, G. R., J. Qian, J. M. C. Plane, P. J. Espy, M. J. Taylor, D. N. Turnbull, and R. P. Lowe, Dynamical and chemical aspects of the mesospheric Na 'wall' event on 9 October 1993 during the ALOHA campaign, *J. Geophys. Res.*, In Press, 1998.

Taylor , M. J., M. A. Hapgood, and P. Rothwell, Observations of gravity wave propagation in the OI (557.7 nm), Na(589.2 nm) and near infrared OH nightglow emission, *Planet. Space Sci.*, **35**, 413-427, 1987.

Taylor, M. J., D. C. Fritts, and J. R. Isler, Determination of horizontal and vertical structure of an unusual pattern of short period gravity waves imaged during ALOHA-93, *Geophys. Res. Lett.*, **22**, 2837-2840, 1998.

Vincent, R. A., Gravity-wave motions in the mesosphere, *J. Atmos. Terr. Phys.*, **46**, 119-128, 1984.

G. R. Swenson and A. Z. Liu, Department of Electrical and Computer Engineering, 313 CSRL, University of Illinois, 1308 West Main Street, Urbana, IL 61801. (email: swenson1@uiuc.edu; liuzr@uiuc.edu)

(Received August 19, 1997; revised December 23, 1997; accepted December 29, 1997.)